Lasers in Surgery and Medicine 35:269–275 (2004)

In Vivo Optical Coherence Tomography for the Diagnosis of Oral Malignancy

Petra Wilder-Smith, DDS, PhD,[1]* Woong-Gyu Jung, MSc,[1] Matthew Brenner, MD,[2] Kathryn Osann, PhD,[2] Hamza Beydoun, BS,[1] Diana Messadi, DDS, DMSc,[3] and Zhongping Chen, PhD[1]

[1]*Beckman Laser Institute, University of California, Irvine, California 92612*

[2]*University of California, Irvine, California 92612*

[3]*University of California, Los Angeles, California 90095*

Background and Objective: Oral cancer results in 10,000 U.S. deaths annually. Improved highly sensitive diagnostics allowing early detection of oral cancer would benefit patient survival and quality of life. Objective was to investigate in vivo non-invasive optical coherence tomography (OCT) techniques for imaging and diagnosing neoplasia-related epithelial, sub-epithelial changes throughout carcinogenesis.

Study Design/Materials and Methods: In the standard hamster cheek pouch model for oral carcinogenesis (n = 36), in vivo OCT was used to image epithelial and sub-epithelial change. OCT- and histopathology-based diagnoses on a scale of 0 (healthy) to 6 (squamous cell carcinoma, SCC) were performed at all stages throughout carcinogenesis by two blinded investigators.

Results: Epithelial, sub-epithelial structures were clearly discernible using OCT. OCT diagnosis agreed with the histopathological gold standard in 80% of readings.

Conclusion: In vivo OCT demonstrates excellent potential as a diagnostic tool in the oral cavity. Lasers Surg. Med. 35:269–275, 2004. © 2004 Wiley-Liss, Inc.

Key words: carcinoma; imaging; leukoplakia; non-invasive diagnostics; oral diagnosis

INTRODUCTION

According to the American Cancer Society, 1,220,100 patients were diagnosed with cancer in the year 2000. In the same year, 552,200 persons were expected to succumb to cancer [1]. Despite significant advances in cancer treatment, early detection of cancer and its curable precursors remains the best way to ensure patient survival and quality of life. Oral cancer will claim approximately 10,000 lives in the U.S. this year [2,3]. Accounting for 96% of all oral cancers, squamous cell carcinoma (SCC) is usually preceded by dysplasia presenting as white epithelial lesions on the oral mucosa (leukoplakia). Leukoplakias develop in 1–4% of the population [2]. Malignant transformation, which is quite unpredictable, develops in 1–40% of leukoplakias over 5 years [2]. Dysplastic lesions in the form of erythroplakias carry a risk for malignant conversion of 90% [2]. Tumor detection is further complicated by a tendency towards field cancerization, leading to multicentric lesions [4]. Current techniques require surgical biopsy of lesions. Benign lesions are often biopsied, reducing patient motivation to agree to further diagnostic biopsies in the future. Conversely, many lesions are only detected by biopsy at an advanced stage, when treatment options and outcome are far from optimal. Of all oral cancer cases documented by the National Cancer Institute Surveillance, Epidemiology, and End Results Program, advanced lesions outnumbered localized lesions more than 2:1. Five-year survival rate is 75% for those with localized disease at diagnosis, but only 16% for those with cancer metastasis [2,3]. A modality for the direct, non-invasive early detection, diagnosis, and monitoring of oral dysplasia and malignancy and for the screening of high-risk populations is urgently required to identify treatment needs at early, more treatable stages of pathological development. Such multi-use clinical capabilities would be likely to produce a sharp drop in morbidity and mortality due to cancer, with substantial reductions in patient anxiety and suffering as well as treatment cost.

Optical Coherence Tomography (OCT)

OCT is a new high-resolution optical technique that permits minimally invasive imaging of near surface abnormalities in complex tissues. It has been compared to ultrasound scanning conceptually [5]. Both ultrasound and OCT provide real time structural imaging, but unlike ultrasound, which utilizes sound waves, OCT is based on low coherence interferometry, using broadband light to

Contract grant sponsor: CRFA; Contract grant number: 27722; Contract grant sponsor: CRFA; Contract grant number: 30003; Contract grant sponsor: CCRP; Contract grant number: 00-01391V-20235; Contract grant sponsor: NIH; Contract grant number: RO21 CA8752701; Contract grant sponsor: TRDRP; Contract grant number: 71T-0192; Contract grant sponsor: NIH (LAMMP); Contract grant number: RR01192; Contract grant sponsor: DOE; Contract grant number: DE903-91ER 61227; Contract grant sponsor: NIH; Contract grant number: EB-00293 CA91717; Contract grant sponsor: NSF; Contract grant numbers: BES-86924, PMUSA-32598; Contract grant sponsor: University of California; Contract grant sponsor: Irvine Chao Family Comprehensive Cancer Center.

*Correspondence to: Petra Wilder-Smith, DDS, PhD, Beckman Laser Institute, 1002 Health Sciences Road East University of California, Irvine, CA 92612. E-mail: pwsmith@bli.uci.edu

Accepted 30 July 2004
Published online in Wiley InterScience (www.interscience.wiley.com).
DOI 10.1002/lsm.20098

provide cross-sectional high resolution sub-surface tissue images [6,7]. The engineering principles behind OCT have been described previously [8–11]. Broadband laser light waves are emitted from a source and directed toward a beam splitter. One wave from the beam splitter is sent toward a reference mirror with known path length and the other toward the tissue sample. After the two beams reflect off the reference mirror and tissue sample surfaces at varying depths within the sample, respectively, the reflected light is directed back towards the beam splitter, where the waves are recombined and read with a photo detector (Fig. 1). The image is produced by analyzing interference of the recombined light waves. Cross-sectional images of tissues are constructed in real time, at near histologic resolution (approximately 10 μm with the current prototype technology). Previous studies using OCT have demonstrated that the imaging penetration depth suffices to evaluate macroscopic characteristics of epithelial and sub-epithelial structures with potential for near histopathological level resolution and close correlation with histologic appearance [12–14].

While some research has been reported in ophthalmologic, dermatologic, GI, gynecological, cardiac, and other OCT applications [11–29], there is limited information on intra-oral OCT, mainly on the topics of periodontal disease and hard tissue pathology, up to this time [30–33].

The 10-μm resolution of OCT permits in vivo non-invasive imaging of the macroscopic characteristics of epithelial and sub-epithelial structures including: (1) depth and thickness, (2) peripheral margins, and (3) potential histopathological appearance. Thus OCT improves on existing clinical capabilities, particularly for identification of multifocal biopsy sites, for regular monitoring of lesions, and for screening high-risk populations. With tissue penetration depth of 1–3 mm, the imaging range of OCT diagnostics is suitable for the oral mucosa. The normal human oral mucosa is very thin, ranging from 0.2 to 1 mm. In hamsters, it is usually somewhat thicker (up to 2 mm), due to the marked surface keratotic layer.

Goal of these feasibility studies was to determine whether premalignant and malignant transformation can be detected and diagnosed in vivo using non-invasive OCT. Specifically, our aims were to (1) identify to what extent OCT can characterize epithelial and sub-epithelial change during carcinogenesis in the hamster cheek pouch model, and (2) compare these data with histopathological diagnosis and staging and determine diagnostic capability.

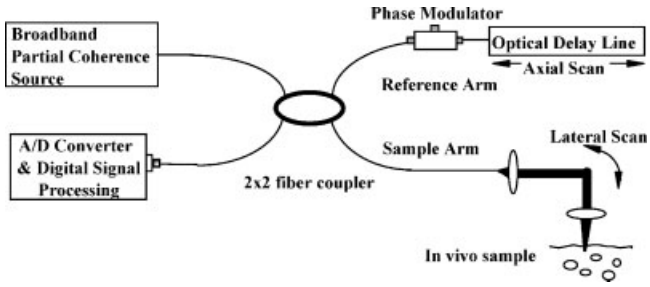

Fig. 1. Schematic of OCT system.

MATERIALS AND METHODS

Animal Model

The standard Golden Syrian Hamster (*Mesocricetus auratus*) cheek pouch model was used. By application of 0.5% DMBA (9,10 dimethyl-1,2-benzanthracene (Sigma, St. Louis, MO) in mineral oil three times per week, mild to severe dysplasia developed at 3–6 weeks, progressing to SCC at 10 weeks. Histological features in this model have been shown to correspond closely with premalignancy and malignancy in human oral mucosa [34]. The study used 36 female animals, 10–12 weeks old. One animal died at 2 days carcinogenesis, leaving a total of 35 animals in this study. To improve study logistics, the animals were randomly divided into three groups of 12 animals each. Only when all the animals from one group had been imaged and sacrificed was the next group was incorporated into the study. The animals were housed and treated in accordance with animal research committee guidelines at the University of California, Irvine (approval 97–1972). The median-lining wall of one cheek pouch of each hamster was treated with carcinogen; the other cheek pouch served as control. Previous studies have shown that this carcinogenesis process in one cheek pouch does not affect the other cheek pouch [35,36], and that therefore the untreated cheek pouch can be used as control.

Protocol

During carcinogenesis over 12 weeks, in vivo (i) clinical evaluation and photography, (ii) high resolution OCT/ODT were performed at weekly intervals. During in vivo measurements, the cheek pouch was continuously irrigated with isotonic saline at room temperature to avoid dehydration. The animals were kept warm using a heating pad and a thermal sock. Use of these measures eliminated animal mortality almost completely during the sometimes lengthy imaging sessions. Only one unplanned animal death occurred throughout the duration of these investigations. Early imaging sessions could last up to 10 minutes; once our techniques were established imaging sessions averaged <3 minutes. The anesthetized hamster's everted cheek pouch was attached to the microscope stage using a specially designed and fabricated ring-shaped clamp fastened rigidly to the stage surface (Fig. 2). The clamping device was marked on its rim at 1-mm intervals to allow the use of localization coordinates for designating areas of specific interest and for achieving repeated, atraumatic scans with different modalities in exactly the same location. Accurate re-localization of the clamping device at weekly intervals was ensured by marking several coordinates of the device outline on the hamster cheek pouch using an animal micro tattooing device (Ketchum lab animal micro tattooer, Ottawa, CDN) at least 7 days prior to the commencement of the study. This time frame was selected as preliminary studies had demonstrated the absence of any tattooing-related tissue changes after a minimum of 5-day post-tattooing. Whilst recognizing the value of tattooing in very close proximity to the area of interest to facilitate the co-localization of corresponding OCT images and

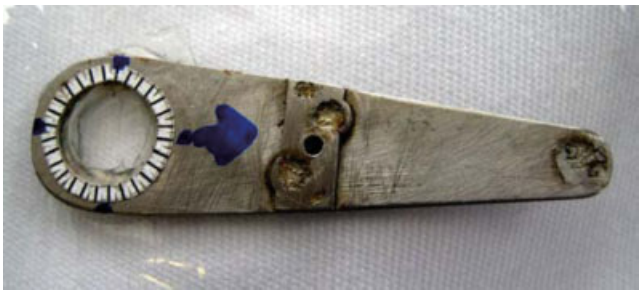

Fig. 2. External fixation device for in vivo OCT and MPM/SHG. 1-mm markings around the periphery provide coordinates for re-localization of lesions at successive imaging sessions. [Figure can be viewed in color online via www.interscience.wiley.com.]

histopathological sections, this technique was not used as other non-invasive imaging techniques at a cellular and sub-cellular level were performed in these animals in addition to OCT. The tattooing process would have affected those results. After optical measurements, one animal from each group was sacrificed each week to obtain specimens for routine paraffin embedding and Hematoxylin and Eosin staining. It was from these 36 animals that the OCT and histopathological data were obtained for evaluation by the diagnostic scorers. A total of 446 OCT images was obtained from the initial total of 36 animals, as both pouches of all living animals were imaged weekly.

OCT

The OCT system used in this study employed a broadband super-luminescent diode laser light source that delivered an output power of 10 mW at a central wavelength of 1,310 nm with a bandwidth of 70 nm. A visible aiming beam (633 nm) was used to find and locate the exact imaging position on the sample. In the reference arm, a rapid-scanning optical delay line was used that employs a grating to control the phase and group delays separately so that no phase modulation was generated when the group delay was scanned [37,38].

The phase modulation was generated through an electro-optic phase modulator that produces a carrier frequency. The axial line scanning rate was 400 Hz, and the modulation frequency of the phase modulator was 500 kHz. Reflected beams from the two arms were recombined in the interferometer and detected on a photodetector. The interference signal was observed only when the optical path length difference between sample and reference arms was less than the coherence length of the source. The detected optical interference fringe intensity signals were bandpass filtered at the carrier frequency. Resultant signals were then digitized with an analog-digital converter and transferred to a computer, where the structural image was generated. The lateral and axial resolutions of the reconstructed image were 10 and 15 μm, respectively.

Histological Evaluation

Histological evaluation of each stained section was quantified by two blinded, pre-standardized scorers (one oral pathologist, one dentist) according to the criteria established by Macdonald [34], whereby each characteristic listed below was assessed. Although a well-defined histological grading system for oral epithelial dysplasia has not been developed yet, most oral pathologists grade on the scale of mild-moderate-severe dysplasia depending on the range and severity of individual features and the proportion of epithelium thickness affected. The following numerical grading system was used for each slide: 0—healthy, 1—hyperkeratosis, 2—mild dysplasia, 3—moderate dysplasia, 4—severe dysplasia, 5—carcinoma-in-situ, and 6—SCC. The criteria for Oral Epithelial Dysplasia were as follows: drop-shaped rete ridges, irregular epithelial stratification, individual cell keratinization, basal cell hyperplasia, loss of intercellular adherence, loss of polarity, hyperchromatic nuclei, increased nucleo-cytoplasmic ratio, anisocytosis, pleomorphic cells and nuclei, abnormal mitotic figures, and increased mitotic activity. Each site was assessed for each of these characteristics at a level of either none (0), slight (1), or marked (2).

OCT Evaluation

The two pre-trained scorers classified each image diagnostically in a blind manner on a scale of 0 (normal) to 6 (SCC). This scale was designed to parallel the scale used for histopathological evaluation [34]. OCT diagnostic scores were based on changes in keratinization, epithelial thickening, epithelial proliferation and invasion, broadening of rete pegs, irregular epithelial stratification, and basal hyperplasia. Epithelial invasion was defined as loss of visible basement membrane. Each site was assessed for each of the above characteristics at a level of either none (0), slight (1), or marked (2). The score for each site depending on the range and severity of individual features and the proportion of epithelial thickness affected.

Data consisted of descriptive images. Scorers were pre-trained using a standard set of 50 OCT and 50 matching histopathological images. Initial training was repeated until at least 98% of images were identified correctly, then 50 new sets of OCT and histopathology images were identified by each scorer with at least 90% accuracy. At this stage, scorers were deemed "pre-standardized" and ready to participate in these studies. Each scorer evaluated all data in one session, which took place once all data accrual was complete. A second re-evaluation of all images by the same scorers in one session, 3 months later, was used to evaluate intra-observer variability

Statistical Evaluation

To test for agreement between the two scorers, and between the same scorer at the first and second evaluation of each sample, a kappa statistic was used. A consensus diagnostic score for any specific image was created by taking the average of the two ratings rounded to the nearest whole integer. The histopathology score was used as the gold standard. Because histopathology was classified into seven different categories, agreement between OCT and histopathology was first described by correlations and percent agreement, then by sensitivity and specificity,

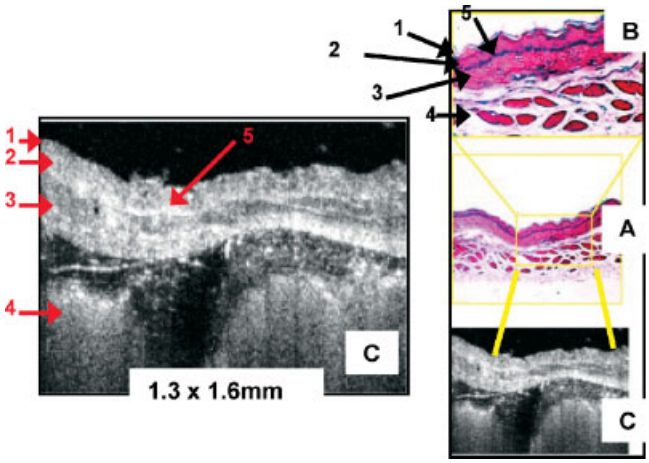

Fig. 3. Healthy cheek pouch H&E stained image (**A**, 20×; **B**, 40×) and in vivo OCT (**C**) of same healthy cheek pouch tissues. Thin normal epithelial and thick sub-epithelial layers are visible. 1—keratinized surface layer, 2—flat stratified squamous epithelium, 3—submucosa: dense fibrous connective tissue, 4—longitudinal striated muscle fiber, and 5—basement membrane.

which are more appropriate for dichotomous discrete variables. The diagnostic sensitivity and specificity of OCT were defined using two approaches: (a) investigating the ability of OCT to differentiate between healthy (0–1) versus pathological (2–6) lesions, and (b) investigating the ability of OCT to differentiate between malignant (5–6) versus non-malignant (0–4) lesions. These values were calculated considering data from each scorer separately (n = 70) and also using the consensus score (n = 35).

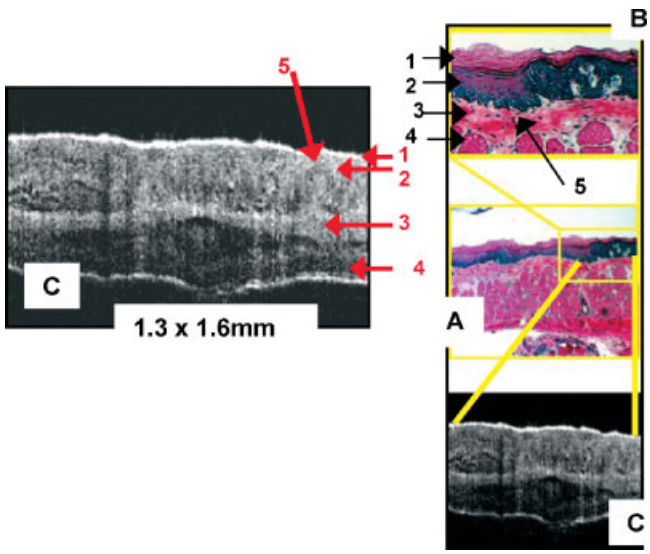

Fig. 4. Dysplastic cheek pouch H&E (**A**, 20×; **B**, 40×): Epithelial thickening, increase in hyperchromatism, pleomorphism of individual cells, loss of polarity in basal cell layer. In vivo OCT (**C**), overall epithelial thickening, broader rete pegs, loss of polarity in basal cell layer. 1—keratinized surface layer, 2—flat stratified squamous epithelium, 3—submucosa: Dense fibrous connective tissue, 4—longitudinal striated muscle fiber, and 5—basement membrane.

RESULTS

The in vivo OCT technology used in these investigations was able to image multiple epithelial and sub-epithelial layers throughout carcinogenesis in the hamster cheek pouch model (Figs. 3–5). Light penetration and image resolution were consistently better in the non-malignant tissues.

The results for diagnosis of each image by two pre-trained investigators are depicted in Table 1. OCT and histopathology were classified into one of seven categories (0 = normal tissue to 6 = SCC). Agreement within scorers, between scorers and between modalities, was assessed using kappa statistics. Intra-observer agreement for the two modalities (histopathology and OCT) at the two scoring timepoints was excellent. Using the kappa statistic for each of the two observers separately and for the observers combined agreement was greater than or equal to 90% for each modality (Table 2).

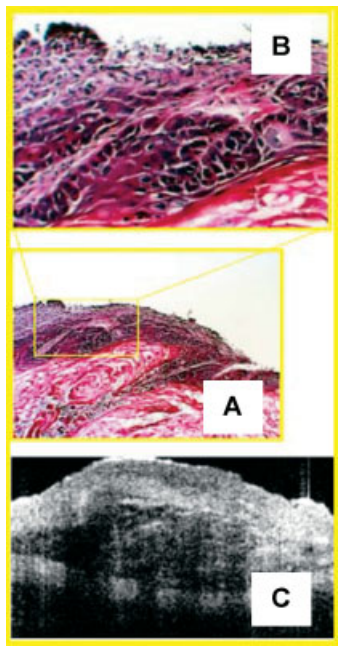

Fig. 5. Malignant cheek pouch. H&E stained image (**A**, 20×; **B**, 40×) and in vivo OCT (**C**) of same cheek pouch with squamous cell carcinoma. In H&E, epithelial pearls are invading the connective tissue. Individual cancer cells exhibit pleomorphism, increased nuclear:cytoplasmic ratio, and hyperchromatism. In OCT, notice loss of normal epithelial stratification and basement membrane. Image definition from sites with SCC was consistently much poorer than from other sites, due to reduced penetration by light into malignant tissues.

TABLE 1. Typical Evaluation Data From 35 Areas, Showing Grading of Pathology on a Scale of 0 (Healthy) to 6 (Squamous Cell Carcinoma), Using H&E Stained Samples and OCT Images

	S1/1	S1/2	S2/1	S2/2	S3/1	S3/2	S4/.1	S4/2	S5/1	S5/2
Histo	0	0	0	0	0	0	0	0	0	0
OCT	0	0	0	0	0	1	0	0	0	0
	S6/1	S6/2	S7/1	S7/2	S8/1	S8/2	S9/1	S9/2	S10/1	S10/2
Histo	1	1	1	1	1	1	1	1	1	1
OCT	0	1	1	1	0	1	1	1	2	1
	S11/1	S11/2	S12/1	S12/2	S13/1	S13/2	S14/1	S14/2	S15/1	S15/2
Histo	2	2	2	2	2	2	2	2	2	2
OCT	2	3	2	2	2	2	1	2	2	2
	S16/1	S16/2	S17/1	S17/2	S18/1	S18/2	S19/1	S19/2	S20/1	S20/2
Histo	3	3	3	3	3	3	3	3	3	3
OCT	3	2	3	3	2	3	4	3	3	3
	S21/1	S21/2	S22/1	S22/2	S23/1	S23/2	S24/1	S24/2	S25/1	S25/2
Histo	4	4	4	4	4	4	4	4	4	4
OCT	5	5	4	4	4	4	4	4	4	4
	S26/1	S26/2	S27/1	S27/2	S28/1	S28/2	S29/1	S29/2	S30/1	S30/2
Histo	5	5	5	5	5	5	5	5	5	5
OCT	5	5	5	5	6	5	6	5	5	5
	S31/1	S31/2	S32/1	S32/2	S33/1	S33/2	S34/1	S34/2	S35/1	S35/2
Histo	6	6	6	6	6	6	6	6	6	6
OCT	6	6	6	5	6	6	6	6	6	6

S1/1 denotes sample one read by scorer 1. S1/2 denotes sample 1 read by scorer 2. Diagnoses were performed by two pre-standardized, blinded investigators. OCT images were kept totally separate from and not matched in any way to histopathological images.

Inter-observor agreement was assessed for both histopathology and OCT. For histopathology, there was perfect agreement between the two scores for any sample. For OCT, there was never a discrepancy of more than 1 point between scorers. The kappa statistic for OCT was 0.603 (SE = 0.091), indicating moderate agreement between observers for scoring.

Overall agreement between readings for OCT and histopathology are illustrated in Table 3. Because histopathology was classified into seven different categories, agreement between OCT and histopathology was first described by percent agreement and the kappa statistic, then by sensitivity and specificity, which are more appropriate for dichotomous discrete variables.

OCT diagnosis agreed with the histopathology for 56 of 70 (80%) readings (kappa = 0.767, SE = 0.056). Using OCT, the histopathology was underestimated by one category in six cases and overestimated in eight cases. In no instance was the difference between histopathology and OCT more than one level. Diagnostic sensitivity of OCT for differentiating between healthy (0–1) versus pathological (2–6) lesions was 0.98 (SE = 0.020) and specificity was 0.95 (SE = 0.049) if each score is considered separately (n = 70). Using this technique, each sample is counted twice, as each sample was evaluated separately by each of the two scorers. Using the consensus score (n = 35) from both investigators (in case of non-consensus, the higher of the two scores was used), sensitivity for OCT was 100% and specificity was 90%.

Diagnostic sensitivity and specificity for differentiating between malignant (5–6) versus non-malignant (0–4) lesions was 100% and specificity was 96% (SE = 0.028). Using the consensus score from both investigators (in case

TABLE 2. Intra-Observer Agreement for Histopathology and OCT at Two Measuring Time Points Separated by a 3-Month Interval

	Histopathology		OCT/ODT	
	Kappa	SE	Kappa	SE
Observer 1	0.933	0.046	0.899	0.056
Observer 2	0.967	0.033	0.900	0.055
Combined	0.950	0.028	0.900	0.039

TABLE 3. Frequencies: OCT (Rows) by Histopathology (Columns)

	0	1	2	3	4	5	6	Total
+							+	
0	9	2	0	0	0	0	0	11
1	1	7	1	0	0	0	0	9
2	0	1	8	2	0	0	0	11
3	0	0	1	7	0	0	0	8
4	0	0	0	1	8	0	0	9
5	0	0	0	0	2	8	1	11
6	0	0	0	0	0	2	9	11
+							+	
Total	10	10	10	10	10	10	10	70

of non-consensus, the higher of the two scores was used), sensitivity for OCT was 100% and specificity was 96%.

DISCUSSION

These studies demonstrate that in vivo OCT can achieve high-resolution images of epithelial and sub-epithelial change, identifying epithelial thickening, as well as changes in stratification and structure.

Inter-observer variability with regard to diagnosis was acceptable, with discrepancies between the evaluators never exceeding 1 point. Scorer consistency was excellent, with repeat evaluations after 3 months showing a kappa equal to or exceeding 90%. Sensitivity was excellent for the diagnosis of SCC, and somewhat reduced for differentiating between different types of dysplasia. As the resolution capabilities of OCT technology are rapidly increasing, their ability to differentiate between different stages of dysplasia should also improve.

Thus, these feasibility studies confirm the usefulness of high-resolution, in vivo OCT imaging as a promising tool for clinical and research needs related to oral premalignancy and malignancy. Further studies are underway to engineer higher resolution systems with improved flexible fiberoptic probe capabilities. These will facilitate the development of new approaches to the clinical diagnosis and management of oral pathologies, and to a better understanding of the processes predicting and paralleling premalignant and malignant change. In future, these capabilities will permit investigation, in patients, into the effects of chemoprevention and chemotherapy on the parameters described above, providing a better understanding of pathological mechanisms, predictors of malignant change in dysplasia, risk of tumor recurrence, and predictors of tumor response to therapy.

REFERENCES

1. American Cancer Society. Cancer facts and figures. In: American Cancer Society Report, 2000. 4 p.
2. Regezi J, Sciubba J, editors. Oral pathology. Philadelphia: W.B. Saunders Co.; 1993. pp 77–90.
3. California Department of Health Services. Cancer Surveillance Section Annual Report, March 1999.
4. Slaughter DP. Field cancerization in oral stratified squamous epithelium. Cancer 1953;6:963–968.
5. Izatt JA, Kobayashi K, Sivak MV, Barton JK, Welch AJ. Optical coherence tomography for biodiagnostics. Opt Photon News 1997;8:41–47.
6. Ding Z. High-resolution optical coherence tomography over a large depth range with an axicon lens. Opt Lett 2002;27:4.
7. Huang D, Swanson EA, Lin CP, Schuman JS, Stinson WG, Chang W. Optical coherence tomography. Science 1991; 254(5035): 1178–1191.
8. Swanson EA, Izatt JA, Hee MR, Huang D, Lin CP, Schuman JS. In vivo retinal imaging by optical coherence tomography. Opt Lett 1993;18(21):1864–1866.
9. Fujimoto JG, Hee MR, Izatt JA, Boppart SA, Swanson EA, Lin CP, et al. Biomedical imaging using optical coherent tomography. Proc SPIE 1999;3749:402.
10. Bouma B, Tearney GJ, Boppart SA, Hee MR, Brezinski ME, Fujimoto JG. High-resolution optical coherence tomographic imaging using a mode-locked Ti:Al/sub 2/O/sub 3/laser source. Opt Lett 1995;20(13):1486–1488.
11. Boppart SA. Optical coherence tomography: Technology and applications for neuroimaging. Psychophysiology 2003;40(4): 529–541.
12. Milner TE, Dave D, Chen Z, Goodman DM, Nelson JS. OCT as a biomedical monitor in human skin. In: Alfano RR, Alfano FJ, editor. Optical coherence tomography. Philadelphia: W.B. Saunders Co.; 1996. pp 220–223.
13. Bamford KJ, James SW, Barr RP, Tatam S. Optical low coherence tomography of bronchial tissue. Advanced materials and optical systems for chemical and biological detection. Proc SPIE 1999;3858:172–179.
14. Pitris C, Jesser C, Boppart SA, Stamper D, Brezinski ME, Fujimoto JG. Feasibility of optical coherence tomography for high-resolution imaging of human gastrointestinal tract malignancies. J Gastroenterol 2000;35:87–92.
15. Bohorfoush AG. New diagnostic methods for esophageal carcinoma. Recent results. Cancer Res 2000;155:55–62.
16. Brand S, Ponero JM, Bouma BE, Tearney GJ, Compton CC, Nishioka NS. Optical coherence tomography in the gastrointestinal tract. Endoscopy 2000;32(10):796–803.
17. Srinivas SM, De Boer JF, Park H, Keikhanzadeh K, Huang HE, Zhang J, Jung WQ, Chen Z, Nelson JS. Determination of burn depth by polarization-sensitive optical coherence tomography. J Biomed Opt 2004;9(1):207–212.
18. Pfau PR, Sivak MV, Jr., Chak A, Kinnard M, Wong RC, Isenberg GA, Izatt JA, Rollins A, Westphal V. Criteria for the diagnosis of dysplasia by endoscopic optical coherence tomography. Gastrointest Endosc 2003;58(2):196–202.
19. Chen Z, Zhao Y, Saxer C, Xiang S, De Boer JF, Nelson JS. Phase-resolved OCT/ODT for imaging tissue microcirculation. Proc SPIE 2000;3915:413–414.
20. Izatt JA, Kulkarni MD, Yazdanfar S, Barton JK, Welch AJ. In vivo bidirectional color Doppler flow imaging of picoliter blood volumes using optical coherence tomography. Opt Lett 1997;22(18):1439–1441.
21. Yazdanfar S, Kulkarni MD, Izatt JA. High resolution imaging of in vivo cardiac dynamics using color Doppler optical coherence tomography. Opt Express 1997;1(13): 14–21.
22. Yazdanfar S, Rollins AM, Izatt JA. In vivo imaging of human retinal flow dynamics by color Doppler optical coherence tomography. Arch Ophthalmol 2003;121(2):235–239.
23. Yonghua Z, Chen Z, Saxer C, Shaohua X, de Boer JF, Nelson JS. Phase-resolved optical coherence tomography and optical Doppler tomography for imaging blood flow in human skin with fast scanning speed and high velocity sensitivity. Opt Lett 2000;25(2):114–116.
24. Patwari P, Weissman NJ, Boppart SA, Jesser C, Stamper D, Fujimoto JG. Assessment of coronary plaque with optical coherence tomography and high-frequency ultrasound. Am J Cardiol 2000;85(5):641–644.
25. Patwari P, Weissman NJ, Boppart SA, Jesser C, Stamper D, Fujimoto JG, Brezinski ME. Assessment of coronary plaque with optical coherence tomography and high-frequency ultrasound. Am J Cardiol 2000;85(5):641–644.
26. Fujimoto JG, Pitris C, Boppart SA, Brezinski ME. Optical coherence tomography: An emerging technology for biomedical imaging and optical biopsy. Neoplasia 2000;2(1–2):9–25.
27. Poneros JM, Brand S, Bouma BE, Tearney GJ, Compton CC, Nishioka NS. Diagnosis of specialized intestinal metaplasia by optical coherence tomography. Gastroenterology 2001; 120(1):7–12.
28. Poneros JM, Tearney GJ, Shiskov M, Kelsey PB, Lauwers GY, Nishioka NS. Optical coherence tomography of the biliary tree during ERCP. Gastrointest Endosc 2002;55(1): 84–88.
29. Feldchtein FI, Gelikonov GV, Gelikonov VM, Kuranov RV, Sergeev AM, Gladkova ND. Endoscopic applications of optical coherence tomography. Opt Express 1998;3(6):123–128.
30. Colston BW, Everett MJ, DaSilva LB, Otis LL, Stroeve P, Nathel H. Imaging of hard and soft tissue in the oral cavity by optical coherence tomography. Appl Opt 1998;37(16):35038.
31. Otis LL, Everett MJ, Sathyam S, Colston BW. Optical coherence tomography: A new imaging technology for dentistry. JADA 2000;131:511–514.
32. Colston BW, Everett MJ, Sathyam US, DaSilva LB, Otis LL. Imaging of the oral cavity using optical coherence tomography. Monogr Oral Sci 2000;17:32–55.

33. Matheny ES, Hanna N, Mina-Araghi R, Jung WG, Chen Z, Wilder-Smith P, Brenner M. Optical coherence tomography of malignant hamster cheek pouches. J Invest Med 2003; 51(1):S78.
34. MacDonald DG. Comparison of epithelial dysplasia in hamster cheek pouch carcinogenesis and human oral mucosa. J Oral Pathol 1981;10:186–191.
35. Wilder-Smith P, Liaw LH, Krasieva TB, Messadi D. Laser-induced fluorescence for detection and diagnosis of oral malignancy. J Dent Res 1999;78:820.
36. Wilder-Smith P, Liaw L-H, Krasieva TB, Nguy L, Yoon Y, Messadi D. Topical ALA-induced fluorescence in oral dysplasia and malignancy. Lasers Surg Med 1999; 69:39.
37. Tearney GJ, Bouma BE, Fujimoto FG. High-speed phase- and group-delay scanning with a grating-based phase control delay line. Opt Lett 1997;22:1811–1813.
38. Rollins AM, Kulkarnis MD, Yazdanfar S, Ung-arunyawee R, Izatt JA. In vivo video rate optical coherence tomography. Opt Express 1998;3:219–229.